Development of Polynuclear Molecular Wires Containing Ruthenium(II) Terpyridine Complexes

Teng-Yuan Dong,* Mei-ching Lin, Michael Yen-Nan Chiang, and Jing-Yun Wu

Department of Chemistry, Center for Nanoscience and Nanotechnology, National Sun Yat-Sen University, Kaohsiung, Taiwan

Received April 12, 2004

The preparations of multinuclear supramolecules assembled from 1′,1‴-bis(terpyridyl)-biferrocene redox-active subunits with Ru^{2+} metal centers are described. The electrochemical measurements of the series of Ru^{2+}-coordinated 1′,1‴-bis(terpyridyl)biferrocene complexes are dominated by the Ru^{2+}/Ru^{3+} redox couple ($E_{1/2}$ at ∼1.35 V), Fe^{2+}/Fe^{3+} redox couples ($E_{1/2}$ from ∼0.4 to ∼0.9 V), and terpy/terpy^{-}/terpy^{2-} redox couples ($E_{1/2}$ at ∼−1.2 and ∼−1.4 V). The appreciable variations detected in the Fe^{2+}/Fe^{3+} oxidation potentials indicate that there is an interaction between the spacer and the Ru^{2+} metal centers. On the coordination of Ru^{2+} metal centers with 1′,1‴-bis(terpyridyl)biferrocene, there is a rise to a red-shifted and more intense $^1[(d(\pi)_{Fe})^6] \rightarrow {}^1[d(\pi)_{Fe})^5(\pi^*_{terpy^{Ru}})^1]$ transition in the visible region. The observed red-shifted absorption from ∼510 nm in monomeric $[Ru(terpy)_2]^{2+}$ and $[Ru(terpy)(fcterpy)]^{2+}$ complexes to ∼570 nm in polynuclear Ru^{2+} 1′,1‴-bis(terpyridyl)biferrocene complexes reveals that there is a qualitative electronic coupling within the array. The coordination of Ru^{2+} transition-metal centers lowers the energy of the π^*_{terpy} orbitals, giving a more red-shifted transition.

Introduction

Recently, the design of new, interesting bis(2,2′:6′,2″-terpyridine) ligands (terpy-terpy) by connecting two terpyridine moieties via a rigid spacer attached to their 4′-positions has received a surge in interest, owing to their utility in the fields of molecular electronics and artificial photosynthesis.[1−5] The terpy-terpy ligands which have been prepared and used further to make dinuclear transition-metal complexes are illustrated in Chart 1.[6−19]

Numerous studies on transition-metal terpy-terpy complexes exhibiting luminescence from metal-to-ligand charge-transfer excited states have been reported. The complexes formed between 2,2′:6′,2″-terpyridine (terpy) and Ru^{2+} are normally only weakly luminescent at room temperature, but attaching a functionalized group at the 4′-position switches on the desired emission. It has been shown that a dinuclear Ru^{2+} terpy-terpy complex substituted with an alkynylene group at the 4′-position can possess a room-temperature luminescence lifetime (τ_p = 565 ns) 1000-fold longer than that of the $Ru(terpy)_2^{2+}$ complex (τ_p = 0.56 ns) in deoxygenated CH_3CN at 25 °C.[12] Furthermore, the energy transfer along the molecular axis can be varied by incorporating additional groups into the alkynylene spacer, and it has been shown that phenyl groups are especially effective at perturbing the electronic properties of the spacer.[12,15,17]

In attempting to perturb the electronic properties of the spacer, we now describe the terpy-bifc-terpy (bifc = biferrocene) system containing redox-active moieties. Ferrocene is a delocalized π-electron ring system of an aromatic molecule. The preparation of 4′-ferrocenyl-2,2′:6′,2″-terpyridine (fcterpy) was reported,[20,21] and cyclic voltammetric measurements of its Ru^{2+} metal com-

(1) Balzani, V.; Scandola, F. *Supramolecular Photochemistry*; Ellis Horwood: Chichester, U.K., 1991.
(2) Sauvage, J.-P.; Collin, J.-P.; Chambron, J.-C.; Guillerez, S.; Coudret, C.; Balzani, V.; Barigolletti, F.; Cloa, L. De; Flamigni, L. *Chem. Rev.* **1994**, *94*, 993.
(3) Collin, J.-P.; Gaviña, P.; Heitz, V.; Sauvage, J.-P. *Eur. J. Inorg. Chem.* **1998**, 1.
(4) Harriman, A.; Ziessel, R. *Coord. Chem. Rev.* **1998**, *171*, 331.
(5) Barigelletti, F.; Flamigni, L. *Chem. Soc. Rev.* **2000**, *29*, 1.
(6) Indelli, M. T.; Scandola, F.; Collin, J.-P.; Sauvage, J.-P.; Sour, A. *Inorg. Chem.* **1996**, *35*, 303.
(7) Patoux, C.; Launay, J.-P.; Beley, M.; Chodorowski-Kimmes, S.; Collin, J.-P.; James, S.; Sauvage, J.-P. *J. Am. Chem. Soc.* **1998**, *120*, 3717.
(8) Beley, M.; Chodorowski-Kimmes, S.; Collin, J.-P.; Lainé, P.; Launay, J.-P.; Sauvage, J.-P. *Angew. Chem., Int. Ed. Engl.* **1994**, *33*, 1775.
(9) Schütte, M.; Kurth, D. G.; Linford, M. R.; Cölfen, H.; Möhwald, H. *Angew. Chem., Int. Ed.* **1998**, *37*, 2891.
(10) Hammarström, L.; Barigelletti, F.; Flamigni, L.; Armaroli, N.; Sour, A.; Collin, J.-P.; Sauvage, J.-P. *J. Am. Chem. Soc.* **1996**, *118*, 11972.
(11) Grosshenny, V.; Harriman, A.; Gisselbrecht, J.-P.; Ziessel, R. *J. Am. Chem. Soc.* **1996**, *118*, 10315.
(12) Benniston, A. C.; Grosshenny, V.; Harriman, A.; Ziessel, R. *Angew. Chem., Int. Ed. Engl.* **1994**, *33*, 1884.
(13) Grosshenny, V.; Harriman, A.; Ziessel, R. *Angew. Chem., Int. Ed. Engl.* **1995**, *34*, 2705.
(14) Grosshenny, V.; Harriman, A.; Ziessel, R. *Angew. Chem., Int. Ed. Engl.* **1995**, *34*, 1100.
(15) El-ghayoury, A.; Harriman, A.; Khatyr, A.; Ziessel, R. *Angew. Chem., Int. Ed. Engl.* **2000**, *39*, 185.
(16) Harriman, A.; Mayeux, A.; De Nicola, A.; Ziesel, R. *Phys. Chem. Chem. Phys.* **2002**, *4*, 2229.
(17) Hissler, M.; El-ghayoury, A.; Harriman, A.; Ziessel, R. *Angew. Chem., Int. Ed.* **1998**, *37*, 1717.
(18) Harriman, A.; Khatyr, A.; Ziessel, R.; Benniston, A. C. *Angew. Chem., Int. Ed. Engl.* **2000**, *39*, 4287.
(19) Barigelletti, F.; Flamigni, L.; Calogero, G.; Hammarström, L.; Sauvage, J.-P.; Collin, J.-P. *Chem. Commun.* **1998**, 2333.
(20) Farlow, B.; Nile, T. A.; Walsh, J. L.; Mcphail, A. T. *Polyhedron* **1993**, *12*, 2891.
(21) Constable, E. C.; Edwards, A. J.; Martinez-Máñez, R.; Raithby, P. R.; Cargill Thompson, A. M. W. *J. Chem. Soc., Dalton Trans.* **1994**, 645.

10.1021/om0497386 CCC: $27.50
Publication on Web 06/30/2004

Chart 1

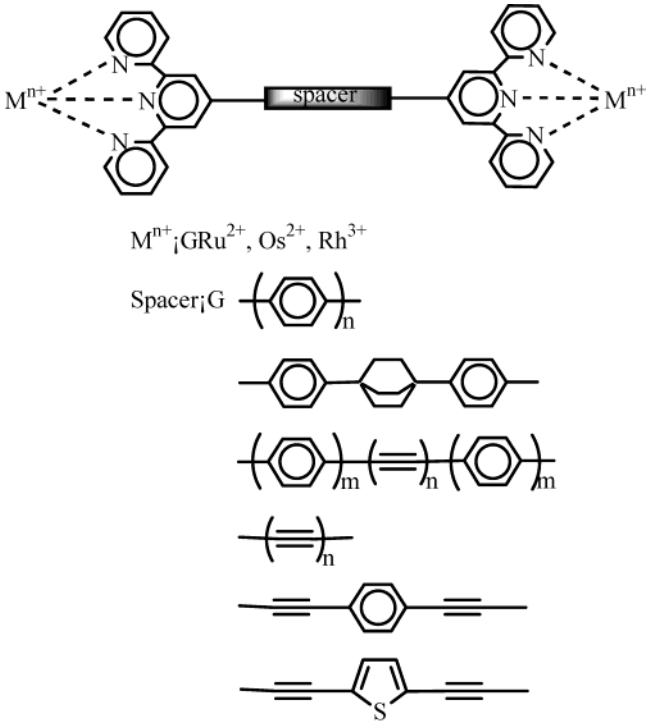

plexes ($[Ru(terpy)(fcterpy)]^{2+}$ and $[Ru(fcterpy)_2]^{2+}$) indicated $Ru^{2+/3+}$ and ferrocenium/ferrocene redox couples at ~ 1.3 and ~ 0.6 V vs Ag/AgCl, respectively.[22] Because electronic coupling between the Ru^{2+} and ferrocenyl center is small, attachment of a ferrocene moiety to the 4′-position of terpy has minimal influence on the electrochemical properties in comparison with the monomeric components.[22] In addition to the $\pi_{terpy}-\pi_{terpy}^*$ absorptions (240−280 nm) and the $d\pi_{Ru}-\pi_{terpy}^*$ MLCT absorption (~480 nm), the $[Ru(terpy)(fcterpy)]^{2+}$ and $[Ru(fcterpy)_2]^{2+}$ complexes exhibit an unusual $^1[(d(\pi)\text{-}fc)^6] \rightarrow {}^1[(d(\pi)fc)^5(\pi^*terpy^{Ru})^1]$ MLCT absorption at ~510 nm.[22] For $[Ru(terpy)(fcterpy)]^{2+}$ and $[Ru(fcterpy)_2]^{2+}$, excited-state lifetime measurements indicated an upper-limit emission lifetime of 25 ns in 4/1 EtOH/MeOH (v/v) at 77 K, substantially shorter than that found for $Ru(terpy)_2^{2+*}$ (τ = 11 μs) at 77 K.[22] The very short lifetime observed for $[Ru(terpy)(fcterpy)]^{2+}$* and $[Ru(fcterpy)_2]^{2+}$* at 77 K is attributed to the presence of a ferrocenyl moiety, which provides additional channels for excited-state decay.

Our interest in the design of materials for applications in molecular electronic wires has focused on how to arrange redox-active subunit controlled transfer of stored information along the wire. Because of the $^1[(d(\pi)\text{-}fc)^6]$ to $^1[(d(\pi)fc)^5(\pi^*terpy^{Ru})^1]$ transition, the binuclear biferrocene appears to be a promising bridge which can ensure fast and quantitative transfer of energy within the array. We recognized that the biferrocene ligand usually employed in mixed-valence chemistry was not readily susceptible to structural variations and would be a very good system for systematic work. Our spectroscopic measurements of mixed-valence biferrocenium have demonstrated that electron transfer in this system is quite facile.[23] Biferrocene exhibits strong interactions between the metal orbitals and the π system of the Cp rings, and electron delocalization could possibly be transmitted by metal−ligand orbital overlap. Because it is relatively easy to oligomerize terpy-bifc-terpy into a long "zigzag" chain, this could be a convenient approach to the preparation of extremely long, photoactive molecular-scale wires. The present paper describes the first step in preparations of multinuclear complexes assembled from a 1′,1″-bis(terpyridyl)biferrocene redox-active subunit attached to ruthenium(II) centers and concentrates on the spectroscopic properties of the simplest diruthenium complexes.

Experimental Section

General Information. All manipulations involving air-sensitive materials were carried out by using standard Schlenk techniques under an atmosphere of N_2. Solvents were dried as follows: THF and ether were distilled from Na/benzophenone; DMF and CH_2Cl_2 were distilled from CaH_2; TMEDA was distilled from KOH. Samples of 1′,1‴-dibromobiferrocene,[24] $Ru(terpy)Cl_3$,[25] $Ru(DMSO)_4Cl_2$,[26] and $Ru(fcterpy)Cl_3$[20,21,27] were prepared according to the literature procedures. As shown in Schemes 1−3, bifcterpy and terpy-bifc-terpy Ru^{2+} complexes can be prepared by using terpy-containing precursors.

Biferrocene-1′-carbaldehyde (1) and Biferrocene-1′,1‴-dicarbaldehyde (2). A sample of 1′,1‴-dibromobiferrocene (1.8 g, 3.41 mmol) was placed in a freshly oven-dried three-necked flask. Dried THF (30 mL) and *n*-butyllithium (4.5 mL, 1.6 M in hexane) were added at −78 °C under N_2. Dried DMF (0.5 mL, 6.5 mmol) was then added at 0 °C, and the solution was further stirred at room temperature for 2 h. Aqueous $Na_2S_2O_3$ solution was added, and the resulting mixture was extracted with CH_2Cl_2. The combined extracts were dried over $MgSO_4$ and evaporated under reduced pressure. The residue was chromatographed on activity III Al_2O_3. The first band that eluted with hexane was the starting material. The second band that eluted with hexane/CH_2Cl_2 (1/1) was biferrocene-1′-carbaldehyde (**1**). The yield was approximately 28%. The physical properties of **1** are as follows. ^1H NMR ($CDCl_3$): δ 3.96 (s, 5H, Cp), 4.20 (dd, 2H, Cp), 4.27 (dd, 2H, Cp), 4.33 (dd, 2H, Cp), 4.39 (dd, 2H, Cp), 4.43 (dd, 2H, Cp), 9.74 (s, 1H, CHO). Mass spectrum (EI, 40 eV): M^+ at *m*/*z* 398. Anal. Calcd for $C_{21}H_{18}Fe_2O\cdot H_2O$: C, 60.62; H, 4.84. Found: C, 61.34; H, 4.41. Continued elution afforded biferrocene-1′,1‴-dicarbaldehyde (**2**). The sample of **2** was obtained in 61% yield. ^1H NMR ($CDCl_3$): δ 4.33 (t, 4H, Cp), 4.38 (t, 4H, Cp), 4.43 (t, 4H, Cp), 4.57 (t, 4H, Cp), 9.7 (s, 2H, CHO). Mass spectrum (EI, 40 eV): M^+ at *m*/*z* 426. Anal. Calcd for $C_{22}H_{18}Fe_2O_2\cdot H_2O$: C, 59.50; H, 4.54. Found: C, 59.83; H, 4.24.

Preparation of Compound 3. 2-Acetylpyridine (0.8 mL, 7.14 mmol) was added to a solution of **1** (2.60 g, 6.53 mmol) in CH_2Cl_2 (10 mL) and ethanol (70 mL). After 2 min, aqueous NaOH (2 M, 15 mL) was added and the mixture was stirred for 2 h. After the addition of water, the mixture was extracted with CH_2Cl_2. The combined extracts were dried over $MgSO_4$ and evaporated under reduced pressure. The residue was chromatographed on activity III Al_2O_3. The first band that eluted with CH_2Cl_2 yielded the starting material. Continued

(22) Hutchison, K.; Morris, J. C.; Nile, T. A.; Walsh, J. L.; Thompson, J. R.; Petersen, J. D.; Schoonover, J. R. *Inorg. Chem.* **1999**, *38*, 2516.

(23) Dong, T.-Y.; Chang, L. S.; Lee, G. H.; Peng, S. M. *Organometallics* **2002**, *21*, 4197 and references therein.

(24) Dong, T.-Y.; Chang, C. K.; Lee, S. H.; Lai, L. L.; Chiang, Y. N. M.; Lin, K. J. *Organometallics* **1997**, *16*, 5816.

(25) Sullivan, B. P.; Calvert, J. M.; Meyer, T. J. *Inorg. Chem.* **1980**, *19*, 1404.

(26) Evans, I. P.; Spencer, A.; Wilkinson, G. *J. Chem. Soc., Dalton Trans.* **1973**, 204.

(27) Butter, I. R.; Mcdonald, S. J.; Hursthouse, M. B.; Abdul Malik, K. M. *Polyhedron* **1994**, *14*, 529.

Scheme 1

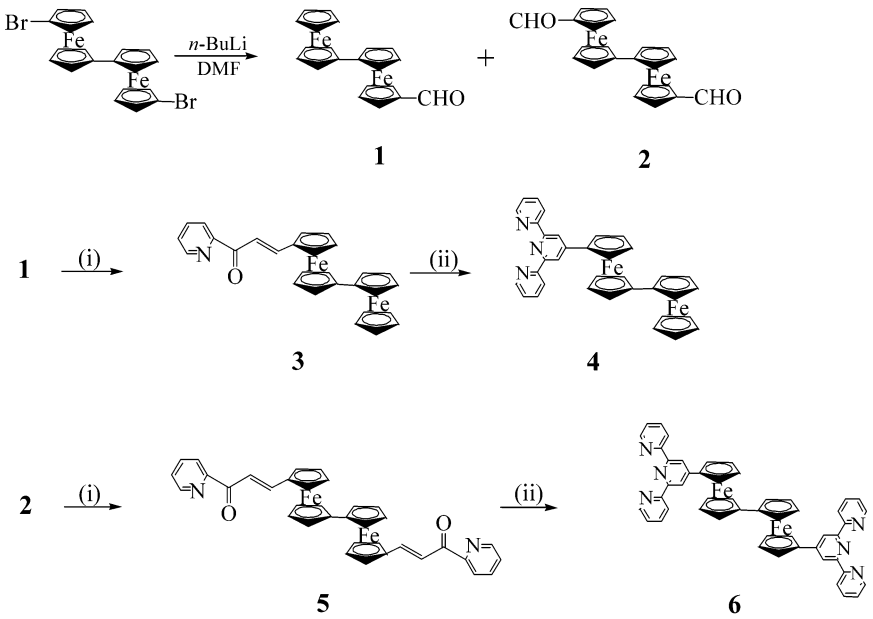

Scheme 2

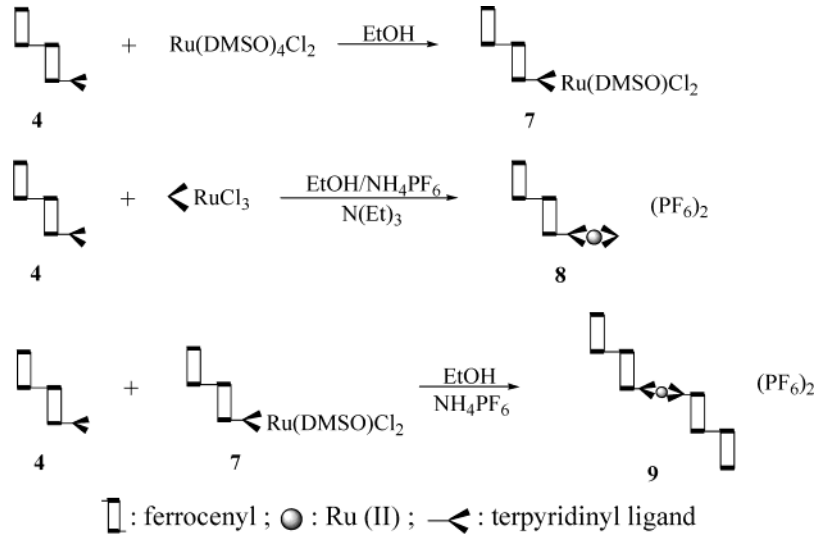

elution with EA/CH_2Cl_2 (1/9) afforded the desired compound **3** (yield 78%). ^{1}H NMR ($CDCl_3$): δ 3.93 (s, 5H, Cp), 4.04 (dd, 2H, Cp), 4.19 (dd, 2H, Cp), 4.27 (dd, 2H, Cp), 4.33 (dd, 2H, Cp), 4.35 (dd, 2H, Cp), 4.47 (dd, 2H, Cp), 7.46 (ddd, 1H, Py), 7.65 (s, 2H, CH=CH), 7.86 (dt, 1H, Py), 8.16 (d, 1H, Py), 8.72 (d, 1H, Py). Mass spectrum (EI, 40 eV): M^+ at *m*/*z* 501.

Preparation of Compound 4. A solution of **3** (0.8 g, 1.60 mmol), 1-(2-pyridinylcarbonyl)pyridinium iodide (0.55 g, 1.69 mmol), and NH_4OAc (~5 g) in ethanol (100 mL) was heated to reflux for 2 h. The solvent was removed under reduced pressure. After the addition of water, the mixture was extracted with CH_2Cl_2. The combined extracts were dried over $MgSO_4$ and evaporated under reduced pressure. The residue was chromatographed on activity III Al_2O_3, with CH_2Cl_2 as eluent. The yield was ~30%. ^{1}H NMR ($CDCl_3$): δ 3.83 (dd, 2H, Cp), 3.84 (s, 5H, Cp), 4.10 (dd, 2H, Cp), 4.13 (dd, 2H, Cp), 4.24 (dd, 2H, Cp), 4.32 (dd, 2H, Cp), 4.83 (dd, 2H, Cp), 7.35 (ddd, 2H, $H_{5,5''}$), 7.88 (dt, 2H, $H_{4,4''}$), 8.28 (s, 2H, $H_{3',5'}$), 8.63 (d, 2H, $H_{3,3''}$), 8.75 (d, 2H, $H_{6,6''}$). Mass spectrum (FAB): M^+ at *m*/*z* 601. Anal. Calcd for $C_{35}H_{27}Fe_2N_3 \cdot H_2O$: C, 67.88; H, 4.72; N, 6.78. Found: C, 68.03; H, 4.67; N, 6.74. Mp: 205−206 °C.

Preparation of Compound 5. 2-Acetylpyridine (0.5 mL, 4.5 mmol) was added to a solution of biferrocene-1′,1‴-dicarbaldehyde (1 g, 2.3 mmol) in CH_2Cl_2 (10 mL) and ethanol (50 mL). After 2 min, aqueous NaOH (2 M, 15 mL) was added and the mixture was stirred for 2 h. After the addition of water, the mixture was extracted with CH_2Cl_2. The combined extracts were dried over $MgSO_4$ and evaporated under reduced pressure. The residue was chromatographed on activity III Al_2O_3. The first and second bands that eluted with CH_2Cl_2 yielded the unknown product and the starting material. Continued elution with EA/CH_2Cl_2 (1/4) afforded the desired compound **5** (yield 64%). ^{1}H NMR ($CDCl_3$): δ 4.00 (t, 4H, Cp), 4.25 (m, 8H, Cp), 4.39 (t, 4H, Cp), 7.43 (ddd, 2H, Py), 7.53 (d, 4H, CH=CH), 7.83 (dt, 2H, Py), 8.14 (d, 2H, Py), 8.69 (d, 2H, Py). Mass spectrum (FAB): M^+ at *m*/*z* 632.

Preparation of Compound 6. A solution of **5** (1.5 g, 2.37 mmol), 1-(2-pyridinylcarbonyl)pyridinium iodide (1.6 g, 4.91

Scheme 3

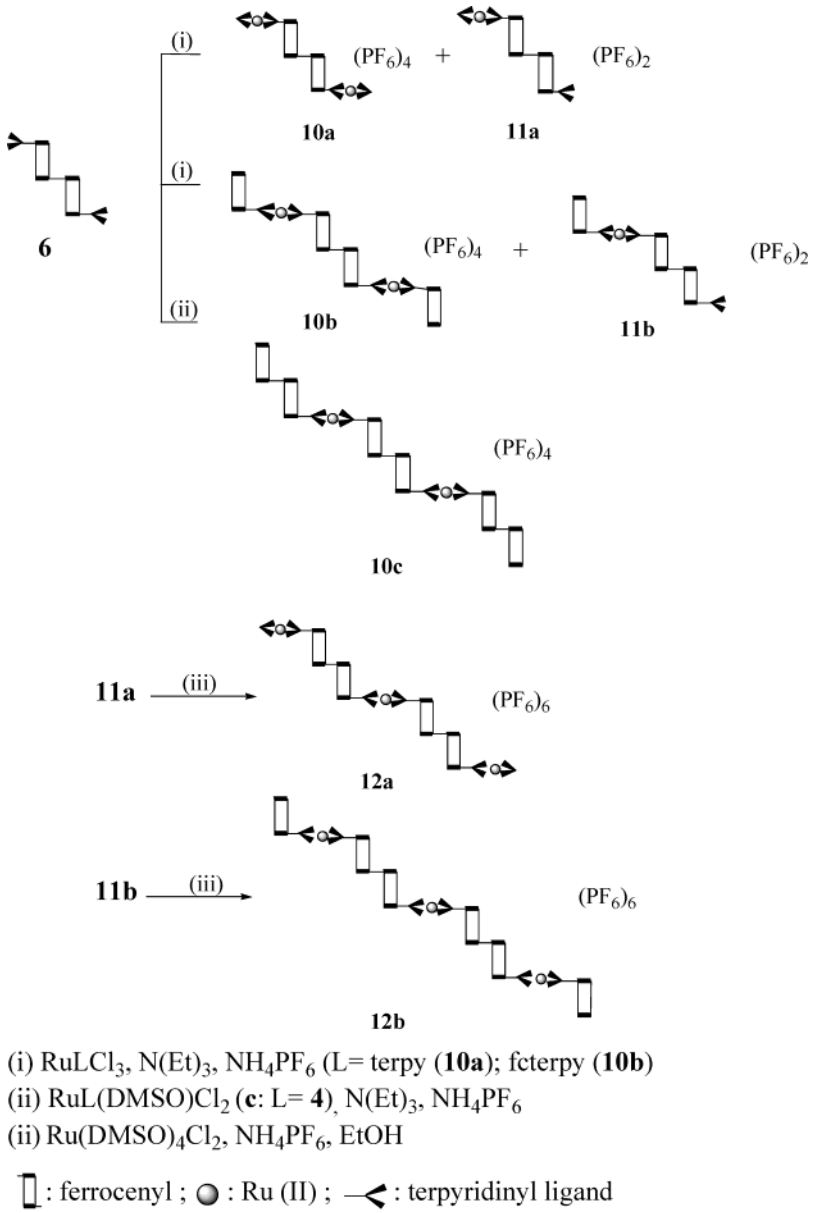

(i) $RuLCl_3$, $N(Et)_3$, NH_4PF_6 (L= terpy (**10a**); fcterpy (**10b**)
(ii) $RuL(DMSO)Cl_2$ (**c**: L= **4**), $N(Et)_3$, NH_4PF_6
(ii) $Ru(DMSO)_4Cl_2$, NH_4PF_6, EtOH

: ferrocenyl ; : Ru (II) ; : terpyridinyl ligand

mmol), and NH_4OAc (~12 g) in ethanol (150 mL) was heated to reflux for 2 h. The solvent was removed under reduced pressure. After the addition of water, the mixture was extracted with CH_2Cl_2. The combined extracts were dried over $MgSO_4$ and evaporated under reduced pressure. The residue was chromatographed on activity III Al_2O_3, with EA/CH_2Cl_2 (1/4) as eluent. The yield was ~18%. ^1H NMR ($CDCl_3$): δ 3.73 (t, 4H, Cp), 3.95 (t, 4H, Cp), 4.18 (t, 4H, Cp), 4.69 (t, 4H, Cp), 7.30 (ddd, 4H, $H_{5,5''}$), 7.83 (dt, 4H, $H_{4,4''}$), 8.13 (s, 4H, $H_{3',5'}$), 8.58 (d, 4H, $H_{3,3''}$), 8.69 (d, 4H, $H_{6,6''}$). Mass spectrum (FAB): $[M + 1]^+$ at *m*/*z* 833. Anal. Calcd for $C_{50}H_{36}Fe_2N_6 \cdot H_2O$: C, 70.59; H, 4.47; N, 9.88. Found: C, 71.07; H, 4.42; N, 9.61. Mp: ~224 °C dec.

Preparation of Ru(bifcterpy)(DMSO)Cl_2 (7). An ethanol solution (10 mL) of $Ru(DMSO)_4Cl_2$ (0.140 g, 0.29 mmol) and bifcterpy (0.180 g, 0.3 mmol) was refluxed for 15 h under N_2. After the mixture was cooled to room temperature, the precipitate was collected by filtration and the crude product was washed with ether several times. The crude product was used without further purification.

Preparation of [Ru(terpy)(bifcterpy)]$(PF_6)_2$ (8). To an ethanol (50 mL) solution of **4** (72 mg, 0.12 mmol) and Ru(terpy)Cl_3 (53.2 mg, 0.12 mmol) was added 3 drops of $N(C_2H_5)_3$ under N_2. The mixture was heated to reflux for 4 h. After the reaction mixture was cooled, the volume of ethanol solvent was reduced by half. An aqueous solution of NH_4PF_6 was added to give a violet-blue precipitate, which was collected by filtration. The crude product was chromatographed on activity V Al_2O_3, and elution with hexane/acetone (3/7) afforded compound **8**. The yield was ~84%. ^1H NMR (d_6-acetone): δ 3.84 (dd, 2H, Cp), 3.89 (s, 5H, Cp), 4.37 (dd, 2H, Cp), 4.54 (dd, 2H, Cp), 4.67−4.69 (dd, 2H, Cp), 5.33 (dd, 2H, Cp), 7.30 (dd, 2H, Py), 7.42 (dd, 2H, Py), 7.64 (d, 2H, Py), 7.78 (dd, 2H, Py), 8.06 (dd, 2H, Py), 8.11 (dd, 2H, Py), 8.47 (dd, 1H, Py), 8.78−8.82 (m, 6H, Py), 9.07 (d, 2H, Py). Mass spectrum (ESI): $[M - PF_6]^+$ *m*/*z* at 1081; $[M - 2PF_6]^{2+}$ *m*/*z* at 468. Anal. Calcd for $C_{50}H_{38}F_{12}Fe_2N_6P_2Ru \cdot H_2O$: C, 48.29; H, 3.24; N, 6.76. Found: C, 48.35; H, 3.48; N, 6.35.

Preparation of [Ru(bifcterpy)$_2$]$(PF_6)_2$ (9). An ethanol (30 mL) solution containing **4** (30 mg, 0.035 mmol) and **7** (22 mg, 0.037 mmol) was heated to reflux under N_2 for 4 h. After the mixture was cooled to room temperature, the volume of ethanol solvent was reduced by half. An aqueous solution of NH_4PF_6 was added to give a violet precipitate, which was collected by filtration. The crude product was chromatographed on activity V Al_2O_3, and elution with acetone afforded compound **9**. The

yield was ~69%. ^{1}H NMR (d_6-acetone): δ 3.84 (dd, 4H, Cp), 3.89 (s, 10H, Cp), 4.38 (dd, 4H, Cp), 4.54 (dd, 4H, Cp), 4.69 (dd, 8H, Cp), 5.33 (dd, 4H, Cp), 7.39 (dd, 4H, Py), 7.72 (dd, 4H, Py), 8.10 (t, 4H, Py), 8.80 (m, 8H, Py). Mass spectrum (ESI): $[M - PF_6]^+$ m/z at 1449; $[M - 2PF_6]^{2+}$ m/z at 652.

Preparation of Compounds 10a−c and 11a−b. An ethanol (40 mL) solution of **6** (50.9 mg, 0.0612 mmol), a stoichiometric amount of the corresponding $RuLCl_3$ (L = 2,2′:6′, 2″-terpyridine, 4′-ferrocenyl- 2,2′:6′,2′-terpyridine) or $RuL(DMSO)Cl_2$ species (L = 4′-biferrocenyl-2,2′:6′,2″-terpyridine), and 10 drops of $N(C_2H_5)_3$ was heated to reflux for 4 h. After the reaction mixture was cooled, the volume of ethanol solvent was reduced by half. An aqueous solution of NH_4PF_6 was added to give a violet-blue precipitate, which was collected by filtration. The crude product was chromatographed on activity V Al_2O_3, with hexane/acetone (1/1) as eluent. The first band was the starting material. Elution with hexane/acetone (3/7) afforded compound **11**. Continued elution with CH_3OH/acetone (5/95) afforded compound **10**. The yield of **10a** was 75%. ^{1}H NMR (d_6-acetone) of **10a**: δ 4.02 (dd, 4H, Cp), 4.57 (dd, 4H, Cp), 4.83 (dd, 4H, Cp), 5.33 (dd, 4H, Cp), 7.29 (dt, 4H, Py), 7.41 (dt, 4H, Py), 7.63 (d, 4H, Py), 7.74 (d, 4H, Py), 8.03−8.07 (ddd, 8H, Py), 8.56 (t, 2H, Py), 8.70 (s, 4H, Py), 8.76 (d, 4H, Py), 8.82 (d, 4H, Py), 9.08 (d, 4H, Py). Mass spectrum of **10a** (ESI): $[M - PF_6]^+$ m/z at 1936; $[M - 2PF_6]^{2+}$ m/z at 895; $[M - 4PF_6]^{4+}$ m/z at 375. Anal. Calcd for **10a** ($C_{80}H_{58}F_{24}Fe_2N_{12}P_4Ru_2 \cdot 2H_2O$): C, 45.37; H, 2.95; N, 7.94. Found: C, 45.36; H, 3.16; N, 7.58. The yield of **10b** was 25%. ^{1}H NMR (d_6-acetone) of **10b**: δ 4.00 (dd, 4H, Cp), 4.35 (s, 10H, Cp), 4.57 (dd, 4H, Cp), 4.80 (dd, 4H, Cp), 4.83 (dd, 4H, Cp), 5.33 (dd, 4H, Cp), 5.52 (dd, 4H, Cp), 7.31 (t, 4H, Py), 7.40 (t, 4H, Py), 7.71 (m, 8H, Py), 8.05 (dd, 8H, Py), 8.70 (s, 4H, Py), 8.78 (d, 4H, Py), 8.97 (d, 4H, Py), 9.19 (s, 4H, Py). Mass spectrum of **10b** (ESI): $[M - 2PF_6]^{2+}$ m/z at 1080; $[M - 3PF_6]^{3+}$ m/z at 672; $[M-4PF_6]^{4+}$ m/z at 467. Anal. Calcd for **10b** ($C_{100}H_{74}F_{24}Fe_4N_{12}P_4Ru_2 \cdot 4H_2O$): C, 47.64; H, 3.23; N, 6.67. Found: C, 47.62; H, 3.02; N, 6.86. The yield of **10c** was 20%. ^{1}H NMR (d_6-acetone) of **10c**: δ 3.85 (dd, 4H, Cp), 3.89 (s, 10H, Cp), 4.38 (dd, 4H, Cp), 4.41 (dd, 4H, Cp), 4.54 (dd, 4H, Cp), 4.58 (dd, 4H, Cp), 4.67 (dd, 4H, Cp), 4.70 (dd, 12H, Cp), 5.32 (dd, 4H, Cp), 5.35 (dd, 4H, Cp), 7.39 (t, 8H, Py), 7.72 (t, 8H, Py), 8.10 (t, 8H, Py), 8.80 (m, 16H, Py). Anal. Calcd for **10c** ($C_{120}H_{90}F_{24}Fe_6N_{12}P_4Ru_2 \cdot 5H_2O$): C, 50.16; H, 3.22; N, 5.97. Found: C, 49.85; H, 3.66; N, 5.24.

Under the condition of stoichiometric amounts (**6**/$RuLCl_3$ = 1/1), the yields of **11a**,**b** can be optimized. Preparation of **11** was carried out in a manner similar to the preparation of **10**. The yield of **11a** was 48%. ^{1}H NMR (d_6-acetone) of **11a**: δ 3.77 (dd, 4H, Cp), 4.02 (dd, 2H, Cp), 4.31 (dd, 2H, Cp), 4.44 (s, 4H, Cp), 4.59 (dd, 2H, Cp), 4.74 (dd, 2H, Cp), 5.22 (dd, 2H, Cp), 7.27 (m, 4H, Py), 7.46 (ddd, 2H, Py), 7.57 (d, 2H, Py), 7.70 (d, 2H, Py), 7.99 (m, 6H, Py), 8.31 (s, 2H, Py), 8.54 (t, 1H, Py), 8.63~8.80 (m, 10H, Py), 9.03 (d, 2H, Py). Mass spectrum of **11a** (FAB): $[M - PF_6]^+$ m/z at 1311 and $[M - 2PF_6]^{2+}$ m/z at 1166. Anal. Calcd for **11a** ($C_{65}H_{47}F_{12}Fe_2N_9P_4Ru \cdot 4.5H_2O$): C, 50.77; H, 3.67; N, 8.19. Found: C, 51.23; H, 3.71; N, 7.69. The yield of **11b** was 30%. ^{1}H NMR (d_6-acetone) of **11b**: δ 3.75 (ddd, 2H, Cp), 4.03 (dd, 2H, Cp), 4.32−4.34 (m, 9H, Cp), 4.45 (d, 2H, Cp), 4.59 (dd, 2H, Cp), 4.75−4.78 (d, 4H, Cp), 5.23 (dd, 2H, Cp), 5.51 (dd, 2H, Cp), 7.28 (dt, 4H, Py), 7.46 (ddd, 2H, Py), 7.67 (d, 2H, Py), 7.95~8.02 (m, 8H, Py), 8.32 (s, 2H, Py), 8.61 (s, 2H, Py), 8.66−8.72 (m, 6H, Py), 8.93 (d, 2H, Py), 9.15 (s, 2H, Py). Mass spectrum of **11b** (ESI-MS): $[M - PF_6]^+$ at m/z 1496, and $[M - 2PF_6]^{2+}$ m/z at 675. Anal. Calcd for **11b** ($C_{75}H_{55}F_{12}Fe_3N_9P_2Ru \cdot 5H_2O$): C, 52.04; H, 3.78; N, 7.28. Found: C, 52.28; H, 3.54; N, 6.81.

Preparation of 12. An ethanol (50 mL) solution of **11** (4 mmol) and a stoichiometric amount of $Ru(DMSO)_4Cl_2$ (2 mmol) were heated to reflux overnight. After the reaction mixture was cooled to room temperature, the volume of ethanol solvent was reduced by half. An aqueous solution of NH_4PF_6 was added to give a violet-red precipitate, which was collected by filtration. The crude product was chromatographed on activity V Al_2O_3. Elution with acetone afforded the starting material. Continued elution with methanol/acetone (5/95) afforded compound **12**. Continued elution with CH_3OH/acetone (5/95) afforded compound **10**. The yield of **12a** was 47%. ^{1}H NMR (d_6-acetone): δ 4.02 (s, 8H, Cp), 4.59 (d, 8H, Cp), 4.83 (dd, 8H, Cp), 5.33 (dd, 8H, Cp), 7.29 (t, 4H, Py), 7.30−7.42 (dt, 8H, Py), 7.64 (ddd, 8H, Py), 7.74 (d, 4H, Py), 8.02−8.08 (m, 12H, Py), 8.56 (t, 2H, Py), 8.70−8.86 (m, 20H, Py), 9.07 (d, 4H, Py). Mass spectrum of **12a** (ESI): $[M - 2PF_6]^{2+}$ m/z at 1506; $[M - 3PF_6]^{3+}$ m/z at 956; $[M - 4PF_6]^{4+}$ m/z at 680; $[M - 5PF_6]^{5+}$ m/z at 516. The yield of **12b** was 35%. ^{1}H NMR (d_6-acetone): δ 4.02 (s, 8H, Cp), 4.33 (s, 10H, Cp), 4.57 (s, 8H, Cp), 4.82 (s, 8H, Cp), 4.89 (s, 4H, Cp), 5.32 (s, 8H, Cp), 5.50 (s, 4H, Cp), 7.32 (m, 12H, Py), 7.71 (m, 12H, Py), 8.06 (m, 12H, Py), 8.70 (m, 12H, Py), 8.94 (d, 8H, Py), 9.19 (s, 4H, Py). Mass spectrum of **12b** (ESI): $[M - 3PF_6]^{3+}$ m/z at 1079; $[M - 4PF_6]^{4+}$ m/z at 773; $[M - 6PF_6]^{6+}$ m/z at 467.

Physical Methods. The ^{57}Fe Mössbauer spectra were run on a constant-acceleration instrument which has been previously described. ^{1}H NMR spectra were run on a Varian INOVA 500 MHz spectrometer. Mass spectra were obtained with a VG-BLOTECH-QUATTRO 5022 system, and ESI-LCQ mass spectra were obtained with a Thermo Finnigan spectrometer. UV spectra were recorded from 250 to 800 nm in CH_3CN by using 1.0 cm quartz cells with a Hitachi U-3591 spectrophotometer. Electrochemical measurements were carried out with a BAS 100W system. Cyclic voltammetry was performed with a stationary glassy-carbon working electrode. These experiments were carried out with a 1×10^{-3} M solution of biferrocene in CH_2Cl_2/CH_3CN (1/1) containing 0.1 M of $(n\text{-}C_4H_9)_4NPF_6$ as supporting electrolyte. The potentials quoted in this work are relative to a Ag/AgCl electrode at 25 °C. Under these conditions, ferrocene shows a reversible one-electron redox wave ($E_{1/2}$ = 0.46 V).

The single-crystal X-ray determinations of compounds **4** and **6** with Mo Kα radiation were carried out at 298 K by using a Rigaku AFC7S diffractometer. An empirical absorption correction based on azimuthal scans of several reflections was applied. The structures were solved by an expanded Fourier technique. All non-hydrogen atoms were refined anisotropically. Hydrogen atoms were included (0.95 Å) but not refined. Complete tables of bond distances and angles and thermal parameters of these compounds are given in the Supporting Information.

Structure Determination of 4. A red crystal (0.10 × 0.22 × 0.98 mm) was grown when a layer of hexane was allowed to slowly diffuse into a CH_2Cl_2 solution of **4**. Data were collected to a maximum 2θ value of 26.0°. Of the 4893 unique reflections (R_{int} = 0.020) collected, there were 2470 with $F_o^2 > 3.0\sigma(F_o^2)$.

Structure Determination of 6 with *C2/c* Phase. An orange-red crystal (0.18 × 0.42 × 0.42 mm) was grown when a layer of cyclohexane was allowed to slowly diffuse into a CH_2Cl_2 solution of **6**. Data were collected to a maximum 2θ value of 26.0°. Of the 4093 unique reflections (R_{int} = 0.019) collected, there were 2164 with $F_o^2 > 3.0\sigma(F_o^2)$.

Structure Determination of 6 with *Pbca* Phase. A red crystal (0.05 × 0.20 × 0.40 mm) was grown when a layer of hexane was allowed to slowly diffuse into a CH_2Cl_2 solution of **6**. Data were collected to a maximum 2θ value of 26.0°. Of the 4289 unique reflections (R_{int} = 0.013) collected, there were 1730 with $F_o^2 > 3.0\sigma(F_o^2)$.

Results and Discussion

Molecular Structure of 4. Details of the X-ray crystal data collections and unit-cell parameters are given in Table 1. The molecular structure of **4** is shown in Figure 1a, and selected bond distances and angles

Table 1. Experimental and Crystal Data for the X-ray Structures of 4 and 6

	4	**6** (*Pbca* phase)	**6** (*C2/c* phase)
formula	$C_{35}H_{27}Fe_2N_3$	$C_{50}H_{36}Fe_2N_6$	$C_{50}H_{36}Fe_2N_6$
M_w	601.31	832.57	832.57
cryst syst	monoclinic	orthorhombic	monoclinic
space group	$P2_1/c$	*Pbca*	*C2/c*
a, Å	22.663(3)	18.080(7)	30.477(8)
b, Å	7.700(6)	27.861(4)	7.381(1)
c, Å	16.319(4)	7.613(3)	17.390(2)
β, deg	105.75(1)		99.75(2)
V, Å^3	2741(2)	3835(2)	3855(1)
Z	4	4	4
D_{calcd}, g cm^{-3}	1.457	1.442	1.434
μ, cm^{-1}	10.87	8.02	7.98
λ, Å	0.710 69	0.710 69	0.710 69
$2\theta_{limits}$, deg	52.0	52.0	52.0
transmissn factors	0.8352−1.0000	0.8585−1.0000	0.7727−1.0000
R^a	0.046	0.033	0.030
$R_w{}^b$	0.066	0.036	0.025

^{a} $R = \sum(||F_o| - |F_c||)/\sum|F_o|$. ^{b} $R_w = \sum[(w|F_o| - |F_c|)^2/\sum(wF_o^2)]^{1/2}$.

are given in Table 2. Complete tables of positional parameters, bond distances, and bond angles are given as Supporting Information.

The ORTEP view confirms the molecular structure, with the biferrocenyl group directly linked to the 4′-position of the 2,2′:6′,2″-terpyridine. The biferrocenyl moiety exists in a trans conformation with the two iron ions on opposite sides of the fulvalenide ligand in which the two Cp rings form a dihedral angle of 1.70°. Inspection of the average distances of Fe−C and Fe−Cp (Fe1−C, 2.035(6) Å; Fe1−Cp, 1.642 Å; Fe2−C, 2.030(7) Å; Fe2−Cp, 1.651 Å) indicates that the two metallocenes are in the Fe^{2+} oxidation state. The bonds and angles about the Cp rings vary little, and they are close to those reported for analogous ferrocenes.[28] The two Cp rings associated with Fe1 and Fe2 are nearly parallel, and the dihedral angles are 2.67 and 2.53°, respectively. Furthermore, the two Cp rings associated with Fe1 and Fe2 are staggered, with average staggering angles of 18.4 and 24.9°, respectively. Attachment of a terpy moiety to the 1′-position of biferrocene has minimal influence on the molecular structure in comparison with analogous biferrocene.[24,29]

The 2,2′:6′, 2″-terpyridine group adopts the expected trans-trans conformation about the interannular C23−C26 and C24−C31 bonds.[30,31] The terpyridine group is not completely coplanar and exhibits dihedral angles between the N1−C21−C22−C23−C24−C25 and N2−C26−C27−C28−C29−C20 planes and between the N1−C21−C22−C23−C24−C25 and N3−C31−C32−C33−C34−C35 planes of 4.43 and 6.37°, respectively. The directly bonded Cp ring of the ferrocene group is not coplanar with the central ring of terpyridine but is slightly twisted with a dihedral angle of 16.09°. A direct comparison of important distances and angles was made between **4** and **6** (Table 3).

Molecular Structure of 6. Compound **6** exhibits two crystalline morphologies at room temperature. Red crystals with the *Pbca* phase were grown when a layer of hexane was allowed to slowly diffuse into a CH_2Cl_2 solution of **6**. An ORTEP view of **6** with the *Pbca* phase is shown in Figure 1b and confirms the molecular structure with the ferrocenyl group directly linked to the 4′-position of the 2,2′:6′,2″-terpyridine. The refinement of the structure imposed an inversion center on the biferrocenyl moiety. Thus, the two ferrocenyl moieties are crystallographically equivalent. Data collected in Table 2 are selected bond distances and angles. Inspection of the average distances of Fe−C (2.043(5) Å) and Fe−Cp (1.65 Å) indicates that the two metallocenes are in the Fe^{2+} oxidation state.[28] The two Cp rings in each ferrocenyl moiety are nearly parallel, and

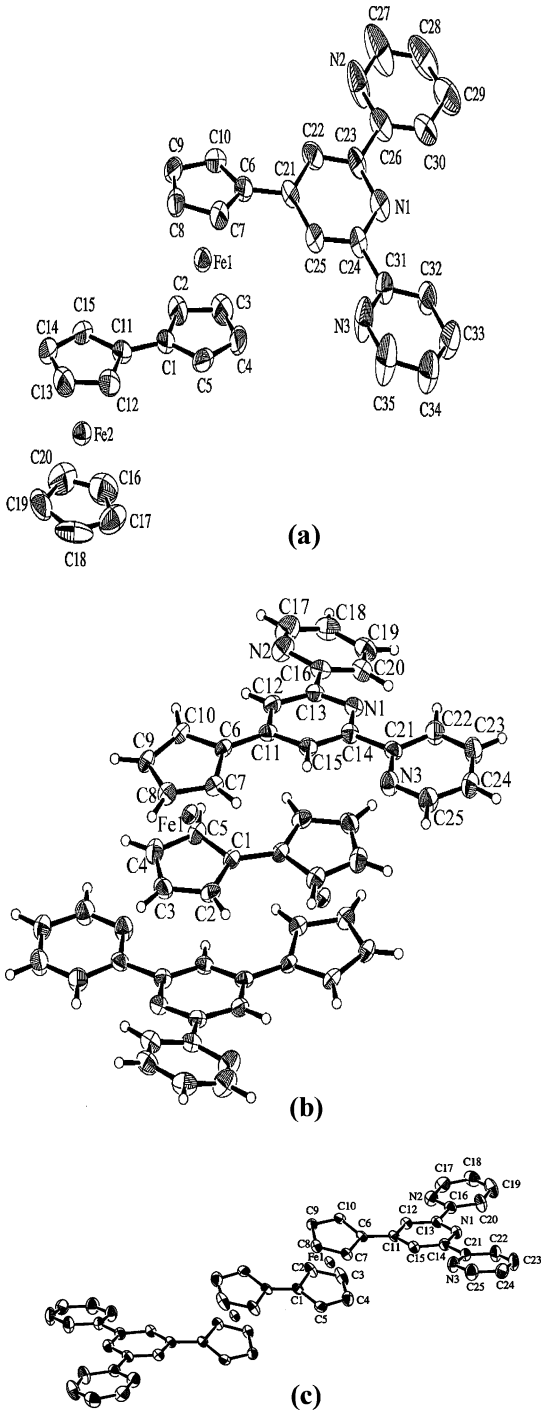

Figure 1. Molecular views of **4** (a), **6** with the *Pbca* phase (b), and **6** with the *C2/c* phase (c).

(28) Seiler, P.; Dunitz, J. D. *Acta Crystallogr., Sect. B* **1979**, *35*, 1068.
(29) Dong, T.-Y.; Ho, P. H.; Lai, X. Q.; Lin, Z. W.; Lin, K. J. *Organometallics* **2000**, *19*, 1096.
(30) Sasaki, I.; Daran, J. C.; Aït-Haddou, H.; Balavoine, G. G. A. *Inorg. Chem. Commun.* **1998**, *1*, 354.
(31) Constable, E. C.; Edwards, A. J.; Marcos, M. D.; Raithby, P. R.; Martïnez-Máñez, R.; Tendero, M. J. L. *Inorg. Chim. Acta* **1994**, *224*, 11.

Table 2. Selected Bond Distances (Å) and Angles (deg) of 4 and 6

	4	**6** (*Pbca*)	**6** (*C*2/*c*)
	Distances		
Fe(1)−C(1)	2.048(5)	2.071(4)	3.128(3)
Fe(1)−C(2)	2.035(6)	2.043(4)	2.033(3)
Fe(1)−C(3)	2.039(6)	2.037(5)	2.017(4)
Fe(1)−C(4)	2.025(6)	2.031(4)	2.031(4)
Fe(1)−C(5)	2.028(6)	2.050(4)	2.042(3)
Fe(1)−C(6)	2.030(5)	2.047(4)	2.039(3)
Fe(1)−C(7)	2.030(5)	2.043(4)	2.031(3)
Fe(1)−C(8)	2.045(6)	2.044(4)	2.051(3)
Fe(1)−C(9)	2.036(6)	2.036(4)	2.051(3)
Fe(1)−C(10)	2.037(6)	2.035(4)	2.027(3)
Fe(2)−C(11)	2.073(5)		
Fe(2)−C(12)	2.058(5)		
Fe(2)−C(13)	2.041(6)		
Fe(2)−C(14)	2.020(6)		
Fe(2)−C(15)	2.022(6)		
Fe(2)−C(16)	2.047(8)		
Fe(2)−C(17)	2.025(8)		
Fe(2)−C(18)	2.014(7)		
Fe(2)−C(19)	2.014(7)		
Fe(2)−C(20)	2.028(7)		
C(6)−C(21)	1.486(8)		
C(23)−C(26)	1.482(9)		
C(24)−C(31)	1.484(8)		
C(6)−C(11)		1.461(5)	1.469
C(13)−C(16)		1.489(6)	1.496(4)
C(14)−C(21)		1.493(5)	1.495(4)
	Angles		
C(25)−C(21)−C(22)	116.5(6)		
C(23)−N(1)−C(24)	117.3(5)		
C(26)−N(2)−C(27)	118.1(8)		
C(31)−N(3)−C(35)	117.8(6)		
C(12)−C(11)−C(15)		116.6(4)	117.2(3)
C(13)−N(1)−C(14)		117.0(4)	117.2(3)
C(16)−N(2)−C(17)		116.7(4)	117.3(3)
C(21)−N(3)−C(25)		117.2(4)	116.9(3)

Table 3. Comparison of Atomic Distances (Å) and Angles (deg)

compd	**4**	**6** (*Pbca*)	**6** (*C*2/*c*)
Fe−C[a]	2.035(6); 2.030(7)	2.043(5)	2.04
Fe−Cp[b]	1.642; 1.651	1.65	1.64
Cp−Cp[c]	2.67; 2.53	2.5	1.33
Cp−Cp[d]	18.4; 24.9	15.5	32.46
Cp−terpy[e]	16.09	11.87	19.19
terpy−terpy[f]	4.43; 6.37	14.52; 9.18	5.96; 6.75

[a] Average Fe−C distance for each ferrocenyl moiety. [b] Distance from the Fe atom to the center of mass of the Cp ring in each ferrocenyl moiety. [c] Dihedral angle between the two least-squares-fitting Cp ring in each ferrocenyl moiety. [d] Average stagger angle between the two Cp rings in each ferrocenyl moiety. [e] Dihedral angle between the Cp ring and the central ring of the terpyridine moiety. [f] Dihedral angle between the central ring and the terminal ring for each terpyridine moiety.

the dihedral angle is 2.5°. Furthermore, the two Cp rings associated with the Fe center are staggered, with an average staggering angle of 15.5°.

The 2,2′:6′,2″-terpyridine group adopts the expected trans-trans conformation about the interannular C13−C16 and C14−C21 bonds.[30,31] The terpyridine group is not completely coplanar and exhibits dihedral angles between the N1−C11−C12−C13−C14−C15 and N2−C16−C17−C18−C19−C20 planes and between the N1−C11−C12−C13−C14−C15 and N3−C21−C22−C23−C24−C25 planes of 14.52 and 9.18°, respectively. The directly bonded Cp ring of the ferrocene group is not coplanar with the central ring of terpyridine but is slightly twisted with a dihedral angle of 11.87°. This degree of nonplanarity is within the range expected for crystal packing effects and represents no significant loss of conjugation between the two rings.

Orange-red crystals with a *C*2/*c* phase were obtained when a layer of cyclohexane was allowed to slowly diffuse into a CH_2Cl_2 solution of **6**. The molecular structure is also shown in Figure 1c, and selected bond distances and angles are given in Table 2. A comparison of important distances and angles was made between **4** and **6** with space groups *Pbca* and *C*2/*c* (Table 3). In the *C*2/*c* phase, the two metallocene moieties are also equivalent. The average Fe−C distance (2.04(3) Å) and the average Fe−Cp distance (1.64(1) Å) indicate that the Fe centers are in the Fe^{2+} oxidation state. The Cp rings in each ferrocenyl moiety are quite parallel with a dihedral angle of 1.33°, and the rings are nearly staggered with an average staggering angle of 32.46(4)°. The 2,2′:6′,2″-terpyridine group adopts the expected trans-trans conformation about the interannular C13−C16 and C14−C21 bonds. The terpyridine group is nearly coplanar and exhibits dihedral angles between the N1−C11−C12−C13−C14−C15 and N2−C16−C17−C18−C19−C20 planes and between the N1−C11−C12−C13−C14−C15 and N3−C21−C22−C23−C24−C25 planes of 5.96 and 6.75°, respectively. However, the directly bonded Cp ring of the ferrocene group is not coplanar with the central ring of terpyridine but is twisted with a dihedral angle of 19.19°.

A comparison of structural features between the two different crystallographic phases of **6** is interesting. The terpy substituent on the Cp ring is situated differently. The two terpy substituents in the *Pbca* phase show a cisoid conformation relative to the fulvalenide ligand. However, in the case of the *C*2/*c* phase, the two terpy substituents show a transoid conformation relative to the fulvalenide ligand. Consequently, the packing arrangements for both phases are different. It appears that the transoid terpy substituents in *C*2/*c* phase lead to further slippage between the molecules. Owing to less steric hindrance between molecules in the *C*2/*c* phase, the terpyridine group is nearly coplanar.

^{57}Fe Mössbauer Measurements. The Mössbauer technique was applied to confirm the oxidation state of Fe centers in the heterogeneous polynuclear transition-metal complexes **10a**−**c**. In general, the ferrocenyl group (electronic ground state $^1A_{1g}$) gives a spectrum characterized by large quadrupole splitting (ΔE_Q) in the range 2.0−2.2 mm s^{-1}, while the spectrum of the ferrocenium cation (electronic groud state $^2E_{2g}$) is characterized by a small or vanishing ΔE_Q value.[23,24] Mössbauer spectra were run for terpyridyl biferrocenes (**4** and **6**) and Ru^{2+}-coordinated complexes (**10a**−**c**). The various absorption peaks in each spectrum were fitted to Lorentzian lines, and the resulting fitting parameters are summarized in Table 4. Representative spectra are also shown in Figure 2. The features in all these spectra include one doublet with $\Delta E_Q = \sim 2.1$ mm s^{-1}. This pattern of one doublet is expected for an iron center in the Fe^{2+} oxidation state.

Electrochemical Results of Free Ligands 4 and 6. Electrochemical data for the Ru^{2+}-uncoordinated terpyridyl biferrocenes **4** and **6**, as well as those for some other relevant compounds, are shown in Table 5. One of the interesting attributes of **4** and **6** is the magnitude of the interaction between the two Fe sites. Cyclic

Table 4. ^{57}Fe Mössbauer Least-Squares Fitting Parameters at 300 K

compd	ΔE_Q[a]	δ[b]	Γ[c]
4	2.306	0.437	0.242, 0.248
6	2.269	0.432	0.228, 0.225
10a	2.129	0.423	0.278, 0.313
10b	2.167	0.439	0.264, 0.283
10c	2.189	0.437	0.270, 0.281

[a] Quadrupole splitting (in mm s^{-1}). [b] Isomer shift (in mm s^{-1}). [c] Full width (in mm s^{-1}) at half-height taken from the least-squares fitting program. The width for the line at more positive velocity is listed first for the doublet.

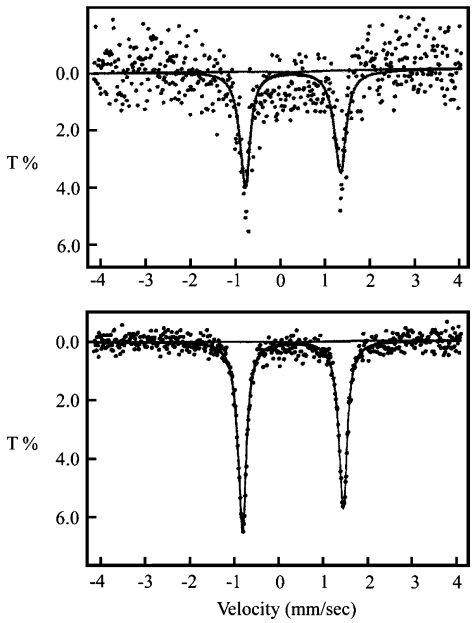

Figure 2. ^{57}Fe Mössbauer spectra of **10a** (top) and **6** (bottom).

voltammetry affords a simple and effective way for estimating this interaction. These binuclear biferrocenes all undergo two successive reversible one-electron oxidations to yield the monocation and the dication. The effect of terpyridyl substitutents on the stability of the Fe^{3+} state is illustrated by the shift of half-wave potentials. The comparison of the half-wave potentials of **4** and **6** with those of biferrocene and 1′,1‴-diethylbiferrocene[32] indicates that the terpyridyl substituent acts as a net electron-withdrawing group.

It has been demonstrated that the magnitude of the peak-to-peak separation ($\Delta E_{1/2}$) gives an indication of the interaction between the two Fe sites in the solution state.[33] A comparison of the magnitude of $\Delta E_{1/2}$ between biferrocene and **6** indicates that the magnitude of interaction between the two Fe sites in the *solution state* in **6** is greater than that in biferrocene. This indicates that the interaction between the two Fe sites is sensitive to the nature of the terpyridyl substituent.

Electrochemical Results of Ru^{2+} Complexes. The electrochemical parameters for **10a**−**c** and related compounds obtained from the CV are summarized in Table 5. As expected, the redox behavior of **10a**−**c** is dominated by the Ru^{2+}/Ru^{3+} redox couple ($E_{1/2}$ at ∼1.35 V), Fe^{2+}/Fe^{3+} redox couples ($E_{1/2}$ from ∼0.4 to ∼0.9 V), and terpy/terpy$^-$/terpy^{2-} redox couples ($E_{1/2}$ at ∼-1.2 and ∼-1.4 V). The Ru^{2+} complex **10a** shows three reversible oxidation processes on sweeping at anodic potentials, corresponding to the oxidation of the biferrocenyl moiety and Ru^{2+}/Ru^{3+} redox couple at 0.61, 0.92, and 1.35 V, respectively. To describe the Fe^{2+}/Fe^{3+} and terpy/terpy$^-$/terpy^{2-} redox couples, the CV voltammograms of **10a**−**c** are shown in Figure 3 in the range from +1.2 to −1.7 V with a scan rate of 100 mV s^{-1}. As shown in Figure 3, two consecutive reduction waves attributed to the reduction of the $Ru(terpy)_2^{2+}$ core appear at −1.16 and −1.43 V. The smaller $\Delta E_{1/2}$ value (0.31 V) of the biferrocenyl moiety as compared to that for the free ligand **6** is expected on the basis of charge buildup after

Table 5. CV Data of 10a−c, 12a,b, and Related Compounds with a Scan Rate of 100 mV s^{-1}

compd	Ru-center	Fe-center		Terpy-center
	$E_{1/2}$ (V)[a]	$E_{1/2}$ (V)[a]	$\Delta E_{1/2}$ (V)[b]	$E_{1/2}$ (V)[a]
ferrocene		0.46		
biferrocene		0.28	0.31	
		0.59		
4		0.45	0.45	
		0.90		
6		0.51	0.43	
		0.94		
	1.36	0.48	0.40	-1.16
		0.88		-1.43
	1.35	0.49	0.39	-1.20
		0.88		-1.45
10a	1.35	0.61	0.31	-1.18
		0.92		-1.42
10b	1.35	0.65	0.28	-1.18
		0.93		-1.42
10c	1.35	0.47	0.40	-1.20
		0.59	0.28	-1.45
		0.87		
12a	1.35	0.61	0.32	-1.16
		0.93		-1.43
12b	1.35	0.62	0.31	-1.18
		0.93		-1.42

[a] All half-wave potentials are referenced to the Ag/AgCl electrode in CH_2Cl_2/CH_3CN (1/1) solution. [b] The difference of $E_{1/2}$ between two redox waves.

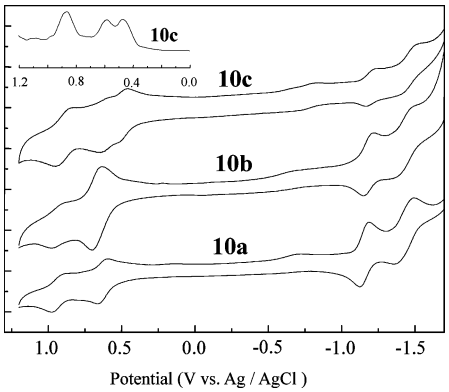

Figure 3. Cyclic voltammograms of **10a**−**c**. The insert shows the DPP for **10c**.

(32) Dong, T.-Y.; Huang, C. H.; Chang, C. K.; Wen, Y. S.; Lee, S. L.; Chen, J. A.; Yeh, W. Y.; Yeh, A. *J. Am. Chem. Soc.* **1993**, *115*, 6359.
(33) (a) Atzkern, H.; Huber, B.; Köhler, F. H.; Müller, G.; Müller, R. *Organometallics* **1991**, *10*, 238. (b) Bunel, E. E.; Campos, P.; Ruz, P.; Valle, L.; Chadwick, I.; Ana, M. S.; Gonzalez, G.; Manriquez, J. M. *Organometallics* **1988**, *7*, 474. (c) Cowan, D. O.; Shu, P.; Hedberg, F. L.; Rossi, M.; Kistenmacher, T. J. *J. Am. Chem. Soc.* **1979**, *101*, 1304. (d) Moulton, R.; Weidman, T. W.; Vollhardt, K. P. C.; Bard, A. J. *Inorg. Chem.* **1986**, *25*, 1846. (e) Obendorf, D.; Schottenberger, H.; Rieker, C. *Organometallics* **1991**, *10*, 1293.

the coordination of the Ru^{2+} ion. In the case of **10b**, the presence of an additional ferrocenyl group does not change the redox potentials appreciably. Three reversible oxidation processes at anodic potentials, corresponding to the oxidations of ferrocenyl and biferrocenyl moieties and the Ru^{2+}/Ru^{3+} redox couple at 0.65, 0.93, and 1.35 V, respectively. Furthermore, two consecutive reduction waves attributed to the reduction of the $Ru(terpy)_2^{2+}$ core at −1.18 and −1.42 V were also observed. The intensity of the process at 0.65 V obtained from differential pulse voltammetry indicates that this process involves the oxidation of the ferrocenyl group and one of the Fe centers of the biferrocenyl group at the same potential. The use of the functionalized 4′-biferrocenyl-2,2′:6′,2″-terpyridine ligand (bifcterpy) in the complex **10c** introduces into the system a new biferrocenyl group. The CV of this complex exhibits four reversible oxidation processes at 0.47, 0.59, 0.87, and 1.35 V. The intensity obtained from differential pulse voltammetry and the comparison of the oxidation potentials indicate that the oxidations of the spacer **6** occur at potentials of 0.59 and 0.87 V. The oxidations of the terminal terpybifc occur at potentials of 0.47 and 0.87 V, which are comparable to the oxidation potentials of the free ligand terpybifc **4** (0.45 and 0.90 V).

Attachment of a biferrocene moiety to the 4′-position of terpy in complexes **10a**−**c**, **8**, and **9** has minimal influence on the Ru^{2+}/Ru^{3+} redox potential (1.35 V), and this observation suggests that the electronic coupling between the Ru^{2+} and terp-bifc-terpy center is possibly rather small. On the other hand, there were appreciable variations detected in the potentials associated with the Fe^{2+}/Fe^{3+} redox couples. The variations of the $\Delta E_{1/2}$ values (0.31 V in **10a**; 0.28 V in **10b**; 0.28 V in **10c**) and the appreciable variations detected in the Fe^{2+}/Fe^{3+} oxidation potentials strongly suggest that there is an interaction between the spacer and the Ru^{2+} centers. Making a comparison for the $E_{1/2}$ values of Fe^{2+}/Fe^{3+} redox couples of **10a**−**c** with free terpybifcterpy (**6**) reveals that there is a qualitative exchange of information within the array. The positive potential shift of the $E_{1/2}$ values for the Fe^{2+}/Fe^{3+} redox couples upon the coordination of the Ru^{2+} ion with free terpybifcterpy ligand **6** indicates that there is an interaction between Ru^{2+} and Fe^{2+} centers. Thus, the terpy-bifc-terpy spacer plays a more sensitive role to gauge the interaction between the Ru^{2+} and Fe^{2+} centers. This is possible due to the existence of weak back-bonding of the Fe^{2+} metal center to the terpy ligand. Furthermore, the decreasing of $\Delta E_{1/2}$ value from 0.43 V in **6** to ∼0.3 V in **10a**−**c** indicates that the magnitude of the Fe−Fe interaction is changed pronouncedly on the coordination of the Ru^{2+} ion. For a symmetrical biferrocene, the smaller value of $\Delta E_{1/2}$ in **10a**−**c** gives an indication of a smaller Fe−Fe interaction.

Furthermore, as shown in Scheme 3, the multinuclear complexes **12a**,**b** assembled from two 1′,1‴-bis(terpyridyl)biferrocene redox-active subunits attached to the Ru^{2+} metal centers can be prepared. Complexes **12a**,**b** also show three reversible redox processes on sweeping at anodic potentials (1.35, 0.93, and 0.61 V for **12a**; 1.35, 0.93, and 0.62 V for **12b**) and two consecutive redox waves attributed to the redox of the $Ru(terpy)_2^{2+}$ core (−1.16 and −1.43 V for **12a**; −1.18 and −1.42 V for **12b**).

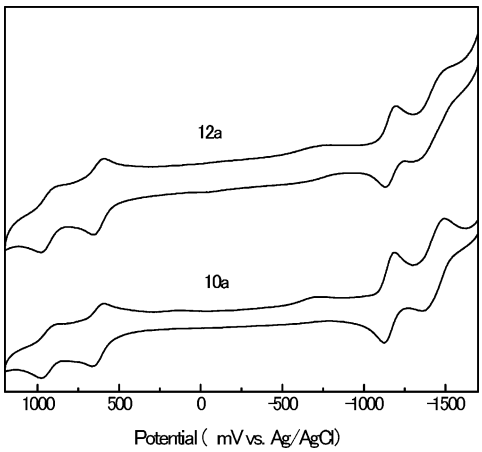

Figure 4. Cyclic voltammograms of **10a** (bottom) and **12a** (top).

Table 6. UV−Visible Absorption Data[a]

compd	abs data, λ_{max}, nm (ϵ, 10^{-3} M^{-1} cm^{-1})
ferrocene	437 (96), 322 (56)
terpyridine	278
fcterpy	459 (0.91), 364 (2.2), 280 (28), 248 (28)
$[Ru(terpy)(fcterpy)][PF_6]_2$[b]	515 (sh), 478 (15), 306 (61), 270 (41)
$[Ru(fcterpy)_2][PF_6]_2$[b]	526 (15), 482 (15), 310 (60), 284 (44), 274 (49)
biferrocene	450 (0.57), 296 (7.90), 269 (8.46)
4	460 (1.3), 355 (sh), 285 (27), 274 (29), 258 (43)
6	481 (4.3), 340 (sh), 281 (99), 276 (104), 272 (99), 253 (130)
10a	568 (16), 483 (53), 308 (200), 270 (174)
10b	578 (27), 489 (33), 313 (131), 283 (119)
10c	570 (33), 485 (40), 311 (170), 280 (162)
8	518 (8.8), 480 (14), 347 (sh), 308 (61), 270 (40), 263 (41)

[a] Acetonitrile solution at room temperature. [b] See ref 22.

As shown in Figure 4, the electrochemical results show no significant difference between **12** and **10**, except for the relative intensity.

UV−Visible Spectroscopy. The UV−visible spectral data of **4**, **6**, **8**, **10a**−**c**, **12a**,**b**, and relevant compounds are summarized in Table 6. The visible absorption bands at 325 nm (ϵ = 51 M^{-1} cm^{-1}) and 440 nm (ϵ = 87 M^{-1} cm^{-1}) of ferrocene have been assigned to the $^1A_{1g} \rightarrow {}^1E_{1g}$ and $^1A_{1g} \rightarrow {}^1E_{2g}$ d−d transitions, respectively.[34−36] In comparison with ferrocene, the absorption band at 450 nm (ϵ = 570 M^{-1} cm^{-1}) for biferrocene are red-shifted, and the molar absorptivity is considerably enhanced. Attachment of a terpy to the biferrocene moiety has a significant influence on the d−d transitions. The visible bands at 460 nm (ϵ = 1300 M^{-1} cm^{-1}) for **4** and at 481 nm (ϵ = 4300 M^{-1} cm^{-1}) for **6** are red-shifted relative to the biferrocene, and the change in molar absorptivity scale with the number of terpy substituents is consistent with the electron-withdrawing character of terpy.[35,36]

As shown in Table 6, the visible spectra for compounds **10a**−**c** are dominated by $^1[(d(\pi))^6] \rightarrow {}^1[d(\pi)^5(\pi^*_{terpy})^1]$ MLCT absorption bands at ∼485 nm, which were assigned by analogy to the well-documented MLCT transitions found for $[Ru(terpy)_2]^{2+}$ (478 nm; ϵ = 14 000

(34) Bhadbhade, M. M.; Das, A.; Jeffery, J. C.; McCleverty, J. A.; Navas Badiola, J. A.; Ward, M. D. *J. Chem. Soc., Dalton Trans.* **1995**, 2769.
(35) Sohn, Y. S.; Hendrickson, D. N.; Gray, H. B. *J. Am. Chem. Soc.* **1971**, *93*, 3603.
(36) Bazak, R. E. *Adv. Photochem.* **1971**, *8*, 227.

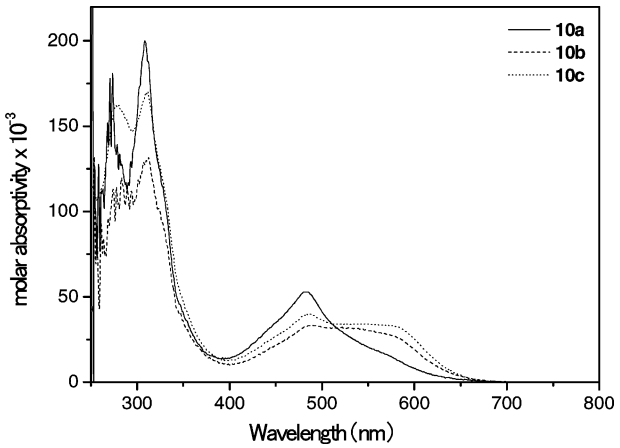

Figure 5. UV−visible absorption spectra of **10a**−**c** in acetonitrile solution at room temperature.

$M^{-1}cm^{-1}$), $[Ru(terpy)(fcterpy)]^{2+}$ (478 nm; ϵ = 15 000 M^{-1} cm^{-1}), and $[Ru(fcterpy)_2]^{2+}$ (482 nm, ϵ = 15 000 M^{-1} cm^{-1}).[22,37−39] The MLCT bands at 483 nm (ϵ = 53 000 M^{-1} cm^{-1}) for **10a**, 489 nm (ϵ = 33 000 M^{-1} cm^{-1}) for **10b**, and 485 nm (ϵ = 40 000 M^{-1} cm^{-1}) for **10c** are slightly red-shifted relative to the monomeric Ru-coordinated compound **8** (480 nm, ϵ = 14 000 M^{-1} cm^{-1}), and the molar absorptivities are considerably enhanced.

As shown in Figure 5, broad structureless absorption bands at 568 nm (ϵ = 16 000 M^{-1} cm^{-1}) for **10a**, 578 nm (ϵ = 27 000 M^{-1} cm^{-1}) for **10b**, and 570 nm (ϵ = 33 000 M^{-1} cm^{-1}) for **10c** are apparent in the visible absorption spectra. In the case of Ru^{2+} transition-metal complexes containing ferrocenyl moieties, an intense broad structureless band in the 520 nm region has been observed.[2,22,40] For the $[Ru(terpy)(fcterpy)]^{2+}$ and $[Ru(fcterpy)_2]^{2+}$ compounds, bands at 515 (sh) and 526 nm (ϵ = 15 000 M^{-1} cm^{-1}) are apparent.[22] This band is assigned to the $^1[(d(\pi)_{Fe})^6] \rightarrow {}^1[d(\pi)_{Fe})^5(\pi^*{}_{terpy}{}^{Ru})^1]$ transition.[2] The intensity of this transition changes with the number of ferrocenyl substituents, and it disappears upon the oxidation of ferrocene. In our studies, this band is not present in the parent compounds (**4** and **6**) but on coordination with Ru^{2+} metal centers in compounds **10a**−**c** rises to a red-shifted and more intense transition in the visible region relative to $[Ru(terpy)(fcterpy)]^{2+}$, $[Ru(fcterpy)_2]^{2+}$, and the monomeric compound **8** (518 nm, ϵ = 8800 M^{-1} cm^{-1}). The observed red-shifted absorption from ∼510 nm in monomeric complexes to ∼570 nm in polynuclear complexes (**10a**−**c**) reveals that there is a qualitative electronic coupling within the array. The coordination of two Ru^{2+} transition-metal centers lowers the energy of the $\pi^*{}_{terpy}$ orbitals, giving a more red-shifted transition.

Conclusion

We have prepared a series of polynuclear redox-active supramolecules with the functionalized 1′,1‴-bis(terpyridyl)biferrocene ligand. Spectroscopic data show that the use of suitable metal ions such as Ru^{2+} will prove to be versatile in building molecular wires. Mössbauer measurements indicate that polynuclear complexes **10a**−**c** are in the Fe(II) oxidation state. The terpy-bifcterpy spacer plays a more sensitive role in gauging the interaction between the Ru^{2+} and Fe^{2+} centers. The positive potential shift of the $E_{1/2}$ values and the decrease in $\Delta E_{1/2}$ value for the Fe^{2+}/Fe^{3+} redox couples upon the coordination of the Ru^{2+} ion with free terpy-bifcterpy ligand **6** indicates that there is an interaction between the Ru^{2+} and Fe^{2+} centers. Furthermore, the observed red-shifted absorption from ∼510 nm in monomeric $[Ru(terpy)_2]^{2+}$ and $[Ru(terpy)(fcterpy)]^{2+}$ complexes to ∼570 nm in polynuclear Ru^{2+} 1′,1‴-bis(terpyridyl)biferrocene complexes reveals that there is a qualitative electronic coupling within the array. The coordination of Ru^{2+} transition-metal centers lowers the energy of the $\pi^*{}_{terpy}$ orbitals, giving a more red-shifted transition. The compound 1′,1‴-bis(terpyridyl)biferrocene potentially has the capability to coordinate transition metals, demonstrating the versatility in molecule assembly and generation of various composites. Expansion of this study to the synthesis of a molecular wire assembled on a gold surface is underway and will be reported in due course.

Acknowledgments are made to the National Science Council (Grant No. NSC92-2113-M-110-011), Taiwan, Republic of China, and the Department of Chemistry and Center for Nanoscience and Nanotechnology at National Sun Yat-Sen University.

Supporting Information Available: Complete tables of positional parameters, bond distances and angles, and thermal parameters for **4**, **6** (*Pbca* phase), and **6** (*C*2/*c* phase). This material is available free of charge via the Internet at http://pubs.acs.org.

OM0497386

(37) Braddock, J. N.; Meyer, T. J. *J. Am. Chem. Soc.* **1973**, *95*, 3158.
(38) Kober, E. M.; Meyer, T. J. *Inorg. Chem.* **1982**, *21*, 3967.
(39) Coe, B. J.; Thompson, D. W.; Culbertson, C. T.; Schoonover, J. R.; Meyer, T. J. *Inorg. Chem.* **1995**, *34*, 3385.
(40) Benniston, A. C.; Goulle, V.; Harriman, A.; Lehn, J.-M.; Marczinke, B. *J. Phys. Chem.* **1994**, *98*, 7798.